Application of Adaptive Autopilot Designs for an Unmanned Aerial Vehicle

Yoonghyun Shin* and Anthony J. Calise†
Georgia Institute of Technology, Atlanta, Georgia, 30332

and

Mark A. Motter‡
NASA Langley Research Center, Hampton, Virginia 23681-2199

This paper summarizes the application of two adaptive approaches to autopilot design, and presents an evaluation and comparison of the two approaches in simulation for an unmanned aerial vehicle. One approach employs two-stage dynamic inversion and the other employs feedback dynamic inversions based on a command augmentation system. Both are augmented with neural network based adaptive elements. The approaches permit adaptation to both parametric uncertainty and unmodeled dynamics, and incorporate a method that permits adaptation during periods of control saturation. Simulation results for an FQM-117B radio controlled miniature aerial vehicle are presented to illustrate the performance of the neural network based adaptation.

Nomenclature

a_n	=	normal acceleration ($a_n = -a_z$)
a_x, a_y, a_z	=	acceleration along the body x, y, and z-axis, respectively
I_{xx}, I_{yy}, I_{zz}	=	moment of inertia in x, y, and z-axis, respectively
P, Q, R	=	rotational rate along the body x, y, and z-axis, respectively
$\delta e, \delta a, \delta r$	=	elevator, aileron, and rudder control deflection, respectively
Δ	=	modeling error
ν	=	pseudo-control

subscripts

c	=	command parameter
s	=	stability axis
h	=	hedging

I. Introduction

Recent technology developments allow unmanned aerial vehicles (UAVs) to displace manned aircraft in many commercial and military roles. As these roles are expanded from simple reconnaissance missions to more complex missions, there is an increasing need for control systems that are robust to model uncertainty due to incomplete modeling, malfunction, or damage during operation. A challenge to designers of flight control systems is to achieve highly maneuverable UAVs without requiring accurate modeling of these vehicles. Adaptive flight control designs provide a way to deal with the uncertainties in the system and environment, without sacrificing performance.

Most UAV developments are based on simple and cheap systems with minimal mass, having minimal or no aerodynamic data for control design. Therefore, control design for UAVs should take these uncertainties into account. UAV dynamics are also significantly affected by their payloads, which can vary depending upon their

* Graduate Research Assistant, School of Mechanical Engineering, gte990x@prism.gatech.edu, Student Member AIAA.
† Professor, School of Aerospace Engineering, anthony.calise@ae.gatech.edu, Fellow AIAA.
‡ Aerospace Engineer, Electronics System Branch, m.a.motter@larc.nasa.gov, Senior Member IEEE.

mission. Therefore, it is highly desirable to employ an approach to flight control design that is low cost and does not require extensive tuning of gain tables. Adaptive approaches to control system design are ideally suited for this application.

This paper will illustrate the use of neural network (NN) based adaptive control designs for a UAV. The main objective of controller design is to demonstrate adaptation to model uncertainties such as unknown or inaccurate mass properties and unknown aerodynamic derivatives, as well as external aerodynamic disturbances such as wind gust that can significantly impact UAV flight performance at low speeds.

This paper presents two NN-based adaptive flight controls that have been successfully utilized for a variety of aerospace applications[1,2,3], incorporating recent advances in the area of state/output feedback and adaptation under saturated control conditions. One approach is based on a two-stage dynamic inversion with approximate feedback linearization and synthesis of a fixed-gain linear compensator, and the other approach is a command augmentation system based dynamic inversion control, while both incorporating NNs as adaptive elements to compensate for the modeling errors, unmodeled dynamic characteristics of the plant[4,5]. The effects of control saturation are also directly accounted for in the design of the adaptive controller through pseudo-control hedging (PCH)[6].

The UAV (FQM-117B) used for this study is described in Section II. A two-stage dynamic inversion based adaptive control design follows in Section III. A command augmentation system based adaptive control design is presented in Section IV. PCH to handle control input nonlinearities is described in Section V, and NNs are briefly discussed in Section VI. Simulation results are presented in Section VII. Conclusions are given in Section IX.

II. The UAV, FQM-117B

The UAV used for this research is the FQM-117B radio controlled miniature aerial vehicle shown in Fig. 1[7,8], which is roughly a 1/9 scale version of Russian fighter aircraft MIG-27. This UAV is composed entirely of injection-molded Styrofoam, and has a 1.70 m wingspan, 1.88 m length, and a total vehicle weight of approximately 6.72 kg. It is powered by a 0.60 cubic inch, 1.9 HP glow fuel engine and has elevator, ruder and full span ailerons. Its moments of inertia are approximately $I_{xx} = 0.2622$, $I_{yy} = 1.2628$, $I_{zz} = 1.5361$, $I_{xz} = -0.0708$, and $I_{xy}=I_{yz} = 0$ kg-m^2.

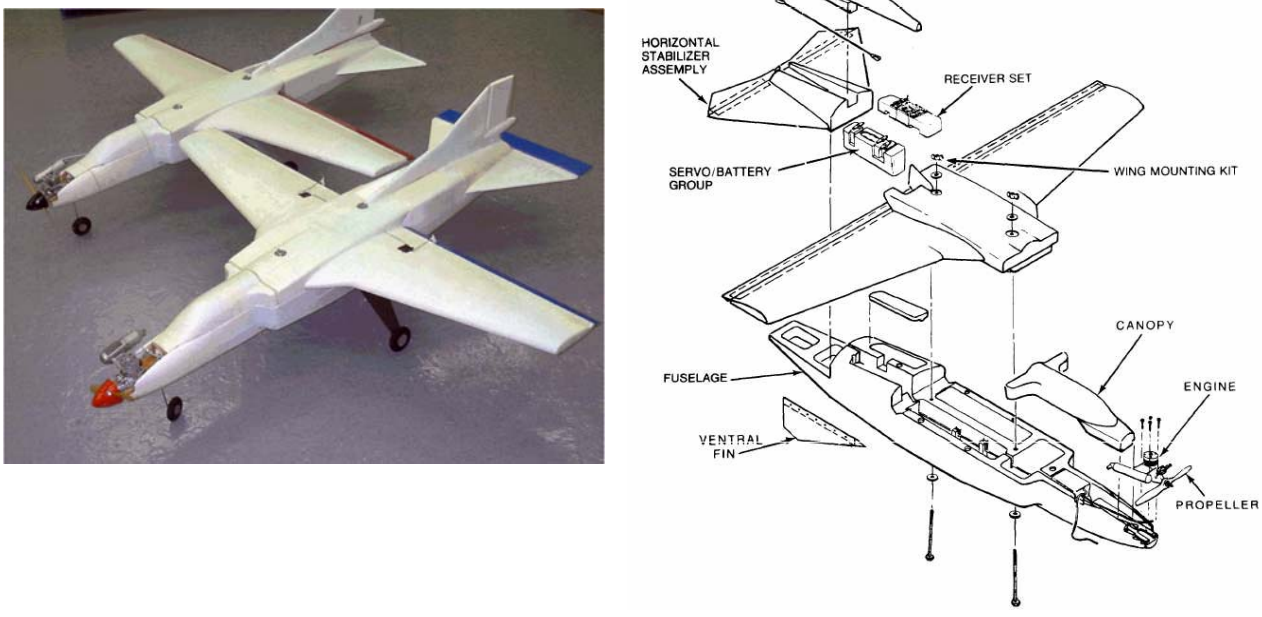

Figure 1. FQM-117B UAV

For the control design of the UAV, only simple static wind tunnel test data were available along with its mass properties. The vehicle employs inexpensive instrumentation, that are noisy and possess a significant amount of bias, drift and scale factor error. In addition, it is clear that its mass property changes significantly as fuel is consumed, and its flight envelope includes low altitude and low speeds where air disturbances such as gust are common.

III. Control Design 1: Two-Stage Dynamic Inversion Based Adaptive Control Design

In this design approach, angle of attack (α), sideslip angle (β) and stability axis roll rate (p_s) are commanded. As shown in Fig. 2, the pilot's command is inputted to the command filters to generate reference signals, while employing pseudo-control hedging (PCH) to protect the adaptive process from effects due to control saturation. Next proportional and derivative (PD) controllers are used to follow the reference commands. The control commands are obtained by a two-stage dynamic inversion. Since there is no α and β sensor, the required feedbacks are assumed to be computed by integration of IMU sensor outputs. The PCH and the NN signals shown in the figure are further discussed in Section V and VI.

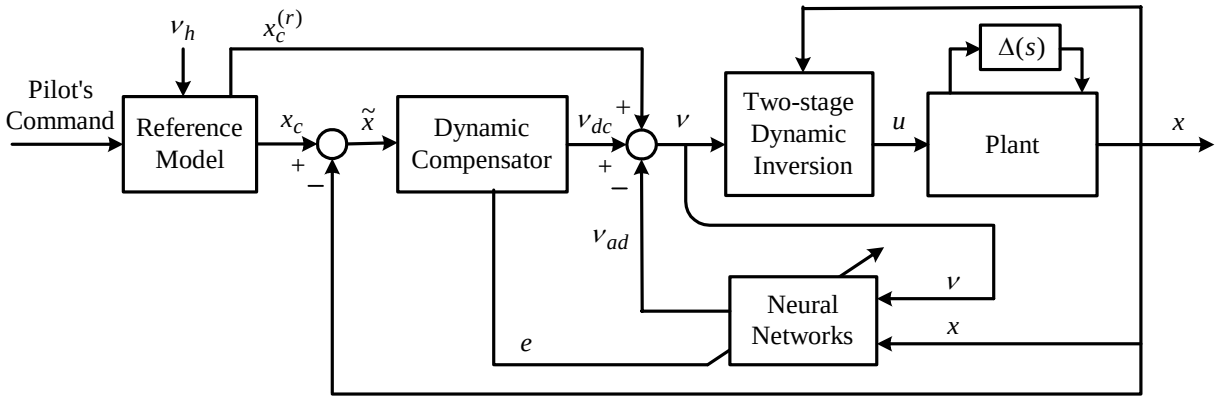

Figure 2. Adaptive feedback control architecture.

A. Two-stage Dynamic Inversion

A two-stage approach for dynamic inversion has been developed for designing a flight control system that regulates $[\, p_s \;\; \alpha \;\; \beta \,]$ [2,9,10,11]. The structure of the inverting law and its implementation is displayed in Fig. 3, where the states for the stage 1 dynamics are $x_1 = [\, \alpha \;\; \dot{\alpha} \;\; \beta \;\; \dot{\beta} \;\; \phi \;\; \theta \;\; V \,]^T$ and those for stage 2 dynamics are $x_2 = [\, p_s \;\; q \;\; r_s \,]^T$.

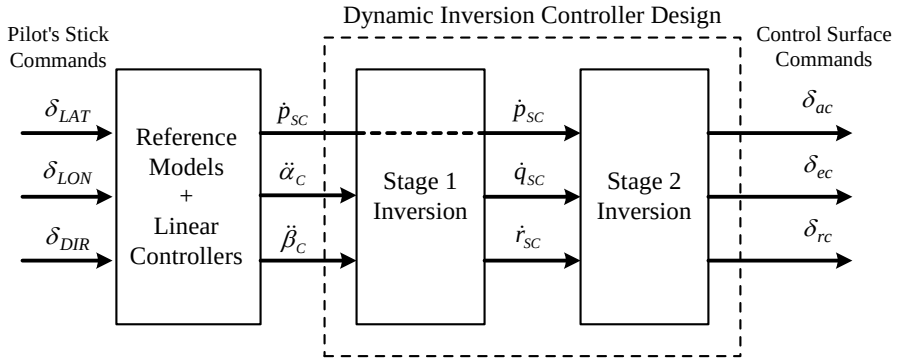

Figure 3. Two-stage dynamic inversion control law structure.

The control variables for the stage 1 dynamics are the angular accelerations in the roll, pitch and yaw stability axis frame, $u_1 = [\dot{p}_{sc} \quad \dot{q}_{sc} \quad \dot{r}_{sc}]^T$ and the control variables for the stage 2 dynamics are the effective control displacement commands in each axis, $u_2 = [\delta_{ac} \quad \delta_{ec} \quad \delta_{rc}]^T$. The regulated variables in each stage are, $y_1 = [p_s, \dot{\alpha}, \dot{\beta}]^T$ and $y_2 = [p_s, q, r_s]^T$. Note that the regulated variables of the stage 1 dynamics are related to regulated variables [p_s α β] according to the relative degree of each regulated variable.

Subject to a set of approximations[14] the stage 1 dynamics can be expressed in the following form

$$\begin{aligned} \begin{bmatrix} \dot{p}_s \\ \ddot{\alpha} \\ \ddot{\beta} \end{bmatrix} &= \begin{bmatrix} 0 \\ f_2(x) \\ f_4(x) \end{bmatrix} + \begin{bmatrix} 1 & 0 & 0 \\ -\tan(\beta) & 1 & 0 \\ 0 & 0 & -1 \end{bmatrix} \begin{bmatrix} \dot{p}_{sc} \\ \dot{q}_c \\ \dot{r}_{sc} \end{bmatrix} \\ &= F(x) + G(x) \cdot u_1 \end{aligned} \tag{1}$$

where p_s and r_s denote the stability axis roll and yaw rates. Similarly, the stage 2 dynamics can be expressed as

$$\begin{bmatrix} \dot{p}_s \\ \dot{q} \\ \dot{r}_s \end{bmatrix} = \begin{bmatrix} f_9(x) \\ f_{10}(x) \\ f_{11}(x) \end{bmatrix} + \begin{bmatrix} L_{\delta a} & 0 & 0 \\ 0 & M_{\delta e} & 0 \\ 0 & 0 & N_{\delta r} \end{bmatrix} \begin{bmatrix} \delta_{ac} \\ \delta_{ec} \\ \delta_{rc} \end{bmatrix} \tag{2}$$

B. Computation of the control

Consider the stage 2 dynamic equation expressed as

$$\begin{aligned} \dot{x}_2 &= A(x) + B(x) \cdot u_2 \\ y_2 &= x_2 \end{aligned} \tag{3}$$

Then it follows that

$$\begin{aligned} \dot{y}_2 &= \dot{x}_2 = A(x) + B(x) \cdot u_2 \\ &= A(x) + B(x) \cdot u_e = u_1 \end{aligned} \tag{4}$$

The stage 1 dynamic equation is given as

$$\dot{y}_1 = F(x) + G(x) \cdot u_1 = \nu \tag{5}$$

where ν is the pseudo control. Combining Eq. (4) and Eq. (5), we have the commanded control that is applied to the aircraft.

$$u = (\hat{G}(x)\hat{B}(x))^{-1}[\nu - \{\hat{F}(x) + \hat{G}(x)\hat{A}(x)\}] \tag{6}$$

where $\hat{G}(x)$, $\hat{B}(x)$, $\hat{F}(x)$ and $\hat{A}(x)$ denote estimates of $G(x)$, $B(x)$, $F(x)$ and $A(x)$.

C. Control Architecture

The pseudo-control for this state feedback control design has the form

$$\nu = x_c^{(r)} + \nu_{dc} - \nu_{ad} \tag{7}$$

where $x_c^{(r)}$ is output of an r^{th}-order reference model that is used to define the desired closed loop response, ν_{dc} is the output of a dynamic compensator, and ν_{ad} is the adaptive signal. The error dynamics for the state feedback can be expressed as

$$\begin{aligned}\tilde{x}^{(r)} &= x_c^{(r)} - x^{(r)} \\ &= -\nu_{dc} + \nu_{ad} - \Delta\end{aligned} \tag{8}$$

It is apparent that the dynamic compensator should be designed to stabilize Eq. (8), and that the role of ν_{ad} is to cancel Δ.

IV. Control Design 2: Command Augmentation Based Adaptive Control Design

As shown in Fig. 4, the acceleration commands to the UAV are first converted to P, Q and R commands (P_c, Q_c, R_c) through an outer-loop controller, while ensuring the vehicle's stability and maintaining trimmed sideslip angle during maneuvers[12]. Then first order reference models are inserted in each channel to generate reference signals, while employing PCH to protect the adaptive process from effects due to control saturation. Next proportional controllers are used to follow the reference commands P_{rm}, Q_{rm} and R_{rm}. The output of the controller is a part of the total pseudo control ν, which is the desired angular acceleration. The equations for angular acceleration are inverted to obtain the effective control in each axis. Figure 4 also shows the NN and the PCH signals, which are further discussed in Section V and VI.

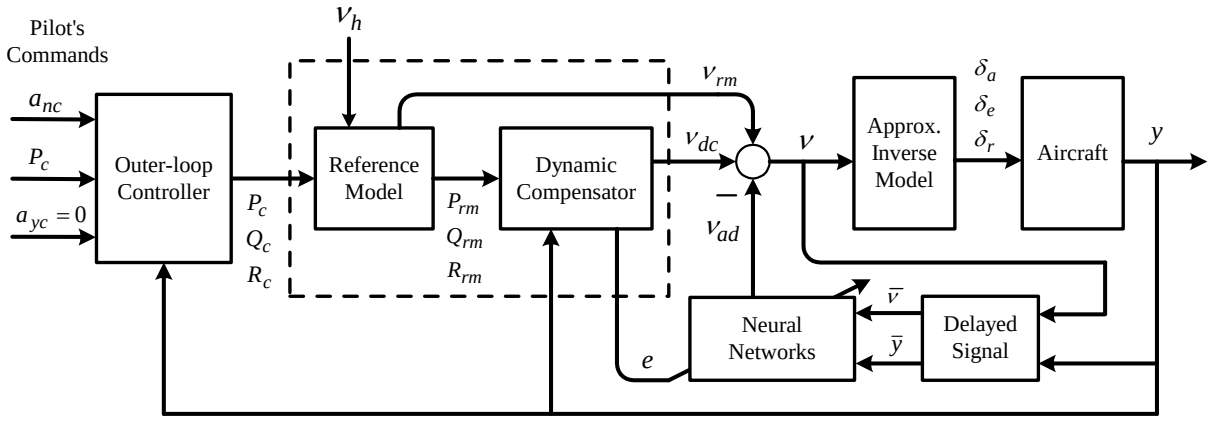

Figure 4. Command augmentation system with NN.

A. Outer-Loop Controller

The outer-loop controller produces a pitch rate command Q_c and a yaw rate command R_c such that the lateral acceleration remains close to zero, which provides turn coordination. The dynamic compensator has a proportional plus integral (PI) form:

$$\begin{aligned}Q_c &= K_1 \cdot (a_{nc} - a_n) + K_2 \cdot \int_0^t (a_{nc} - a_n)\, d\tau \\ R_c &= -K_3 \cdot a_y - K_4 \cdot \int_0^t a_y \, d\tau\end{aligned} \tag{9}$$

where the feedback gains K_1, K_2, K_3, and K_4 can be selected based on speed of response.

B. Command Filter (Reference Model)

A first order reference model is introduced to generate reference signals in each channel. For instance, for roll channel it is

$$\frac{P_{rm}}{P_c} = \frac{1}{\tau \cdot s + 1} \tag{10}$$

where τ is the desired roll mode time constant. In this process, pseudo-control hedging is incorporated to handle control nonlinearities.

C. Dynamic Compensator and Control

The derivatives of the body angular angles can be described as, designating the approximate mathematical models $\hat{\dot{P}}, \hat{\dot{Q}}, \hat{\dot{R}}$ with the pseudo controls, ν_p, ν_q, ν_r:

$$\begin{bmatrix} \hat{\dot{P}} \\ \hat{\dot{Q}} \\ \hat{\dot{R}} \end{bmatrix} = \begin{bmatrix} \nu_p \\ \nu_q \\ \nu_r \end{bmatrix} = \begin{bmatrix} F_1(x) \\ F_2(x) \\ F_3(x) \end{bmatrix} + \begin{bmatrix} G_1 & 0 & 0 \\ 0 & G_2 & 0 \\ 0 & 0 & G_3 \end{bmatrix} \cdot \begin{bmatrix} \delta_a \\ \delta_e \\ \delta_r \end{bmatrix} \tag{11}$$

Inverting Eq. (11) resulting in the control laws:

$$\begin{bmatrix} \delta_a \\ \delta_e \\ \delta_r \end{bmatrix} = \begin{bmatrix} G_1 & 0 & 0 \\ 0 & G_2 & 0 \\ 0 & 0 & G_3 \end{bmatrix}^{-1} \cdot \begin{bmatrix} \nu_p - F_1(x) \\ \nu_q - F_2(x) \\ \nu_r - F_3(x) \end{bmatrix} = \begin{bmatrix} G_1^{-1} \cdot (\nu_p - F_1(x)) \\ G_2^{-1} \cdot (\nu_q - F_2(x)) \\ G_3^{-1} \cdot (\nu_r - F_3(x)) \end{bmatrix} \tag{12}$$

The controls in Eq. (12) are based on the simplified functions $F_i(x)$, i =1,2,3, which retain only a few dominate terms:

$$\begin{aligned} F_1(x) &= \frac{S\bar{q}b}{I_{xx}} C_{lp} \cdot \left(\frac{pb}{2U} \right) + \frac{S\bar{q}b}{I_{xx}} C_{l\beta} \cdot \beta \\ F_2(x) &= \frac{S\bar{q}\bar{c}}{I_{yy}} C_{mq} \cdot \left(\frac{q\bar{c}}{2U} \right) + \frac{S\bar{q}\bar{c}}{I_{yy}} C_{m\alpha} \cdot \alpha \\ F_3(x) &= \frac{S\bar{q}b}{I_{zz}} C_{nr} \cdot \left(\frac{rb}{2U} \right) + \frac{S\bar{q}b}{I_{zz}} C_{n\beta} \cdot \beta \end{aligned} \tag{13}$$

and

$$G_1 = \frac{S\bar{q}b}{I_{xx}} C_{l\delta a}, \; G_2 = \frac{S\bar{q}\bar{c}}{I_{yy}} C_{m\delta e}, \; G_3 = \frac{S\bar{q}b}{I_{zz}} C_{n\delta r} \tag{14}$$

Here the aerodynamic coefficients ($C_{lp}, C_{m\alpha}$, etc) and control effectiveness ($C_{l\delta a}, C_{m\delta e}, C_{n\delta r}$) are set to constant values within reasonable ranges. These approximations introduce modeling error.

The exact expression for $\dot{P}$ can be, for instance, written by

$$\dot{P} = C_l \cdot \frac{S\bar{q}b}{I_{xx}} \tag{15}$$

where

$$C_l = C_{l0} + C_{l\beta} \cdot \beta + C_{l_p} \cdot \frac{pb}{2V} p + C_{l_r} \cdot \frac{rb}{2V} + C_{l\phi} \cdot \delta\phi + C_{l\delta a} \cdot \delta a + C_{l\delta r} \cdot \delta r + \cdots \tag{16}$$

Because only a few dominant terms among those in Eq.(16) are retained in Eq.(11) and (13), there always exists a modeling error Δ_p defined by

$$\Delta_p = \dot{P} - \hat{\dot{P}} = \dot{P} - \nu_p \tag{17}$$

Modeling errors Δ_q and Δ_r in pitch and yaw channels, respectively, can also be defined by the same way. Using these definitions, the time derivatives of angular rates can be described by:

$$\begin{aligned}\dot{P} &= \hat{\dot{P}} + \Delta_p = \nu_p + \Delta_p \\ \dot{Q} &= \hat{\dot{Q}} + \Delta_q = \nu_q + \Delta_q \\ \dot{R} &= \hat{\dot{R}} + \Delta_r = \nu_r + \Delta_r\end{aligned} \tag{18}$$

The equations in Eq.(11) can be transformed to a linear, time invariant form by designating the pseudo-controls including *only* proportional control laws:

$$\begin{aligned}\nu_p &= A_1 \cdot (P_c - P) - \nu_{adp} \\ \nu_q &= A_2 \cdot (Q_c - Q) - \nu_{adq} \\ \nu_r &= A_3 \cdot (R_c - R) - \nu_{adr}\end{aligned} \tag{19}$$

where $\nu_{adp}, \nu_{adq}, \nu_{adr}$ are adaptive signals which are the output of neural networks as shown in Fig. 4. Substitution Eq. (19) into Eq. (18) gives

$$\begin{aligned}\dot{P} &= A_1 \cdot (P_c - P) - \nu_{adp} + \Delta_p \\ \dot{Q} &= A_2 \cdot (Q_c - Q) - \nu_{adq} + \Delta q \\ \dot{R} &= A_3 \cdot (R_c - R) - \nu_{adr} + \Delta_r\end{aligned} \tag{20}$$

Hence, if the NN adaptive signals ($\nu_{adp}, \nu_{adq}, \nu_{adr}$) cancel out the modeling errors ($\Delta_p, \Delta_q, \Delta_r$), then asymptotic tracking in body angular rates can be expected. Consequently, the neural networks play the key role of generating the adaptive signals to compensate for the modeling errors due to the use of approximate models, uncertainties in each channel. Feedback gains A_1, A_2, A_3 are chosen to satisfy the desired handling qualities.

D. Output Feedback Design

Most of UAV implement simple, fundamental measuring instruments, so only a set of limited parameters is usually available for feedback. Thus, an output feedback design of the control system should be considered for such cases.

As a further simplification, one can ignore angle of attack (α) and sideslip angle (β) dependencies, and then the terms including these angle values in Eq.(13) could be omitted, and in addition the *x*-axis speed component, *U* may be replaced by the total speed *V* as shown below:

$$F_1(x) = \frac{S\bar{q}b}{I_{xx}} C_{lp} \cdot \left(\frac{pb}{2V}\right), \quad F_2(x) = \frac{S\bar{q}\bar{c}}{I_{yy}} C_{mq} \cdot \left(\frac{q\bar{c}}{2V}\right), \quad F_3(x) = \frac{S\bar{q}b}{I_{zz}} C_{nr} \cdot \left(\frac{rb}{2V}\right) \tag{21}$$

According to the theoretical background on the adaptive output feedback design presented in Ref. 5, the delayed signals in each channel are input to the NN adaptive elements (see Section VI).

V. Pseudo-Control Hedging (PCH)

PCH is used to address NN adaptation difficulties arising from various actuation nonlinearities, including actuator position and/or rate saturation, discrete (magnitude quantized) control, time delays and actuator dynamics[6]. NN training difficulties occur when unmodeled actuator characteristics are encountered. For example, the NN adaptive element will attempt to adapt to these nonlinearities, even when it is impossible to do so. The goal of PCH is to prevent the adaptive element from attempting to adapt to these characteristics, while not affecting NN adaptation to other sources of inversion error. Conceptually, PCH "moves the reference model backwards" by an estimate of the amount the controlled system did not move due to selected actuator characteristics (such a position and rate limits, time delays, etc). The reference model is hedged according to an estimate of the difference between the commanded and actually achieved pseudo-control.

The hedge signal is defined as

$$\nu_h = \nu - \hat{\nu} \tag{22}$$

where ν is the commanded pseudo control and $\hat{\nu}$ is an estimate for the achieved pseudo control. For the design approach in Section III, for example, ν is defined in Eq. (5) and the estimate is obtained by combining Eq. (3) and (4) and replacing the elements of u_2 in Eq. (4) by estimates obtained from actuator models of the form depicted in Fig. 5. Thus,

$$\nu_h = \nu - [\hat{F}(x) + \hat{G}(x)\hat{A}(x) + \hat{G}(x)\hat{B}(x)\cdot\hat{u}_2] \tag{23}$$

The elements of the hedge signal are then subtracted in the reference models for each respective axis. The manner in which this is done for a second order reference model is depicted in Fig. 6.

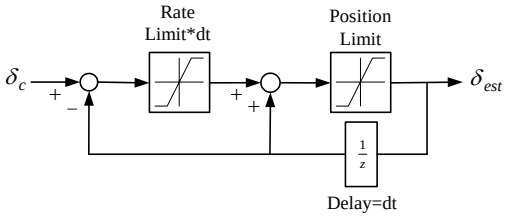

Figure 5. Actuator estimator.

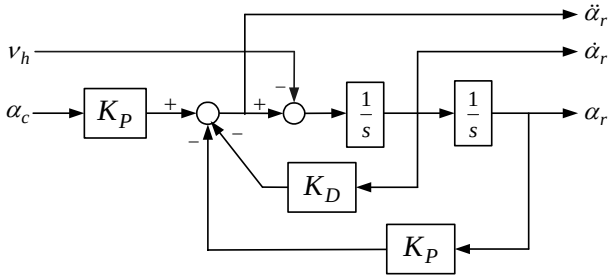

Figure 6. Reference model with hedging in pitch channel.

VI. Neural Network Adaptation

The modeling error Δ depends on the states and the pseudo control. It has been shown that this error can be approximated[5], in a bounded region, to any desired degree of accuracy using a NN with a sufficient number of hidden layer neurons, having the following input vector

$$\mu(t) = [\,1 \quad \bar{\nu}_d^T(t) \quad \bar{y}_d^T(t)\,] \tag{24}$$

where

$$\begin{aligned} \bar{\nu}_d^T(t) &= [\,\nu(t) \quad \nu(t-d) \quad \cdots \quad \nu(t-(n_1-r-1)d)\,]^T \\ \bar{y}_d^T(t) &= [\,y(t) \quad y(t-d) \quad \cdots \quad y(t-(n_1-1)d)\,]^T \end{aligned} \tag{25}$$

with $n_1 \geq n$, $\bar{d} > d > 0$ denoting time delay.

In the case of a single hidden-layer, multi-perceptron NN shown in Fig. 7, we have

$$\nu_{ad} = \hat{W}^T \sigma(\hat{V}^T \mu) \tag{26}$$

where σ is a vector whose elements, $\sigma_i(z_i)$, are the basis functions of the NN. Typically, these basis functions are selected as so-called squashing functions. The form we employed is $\sigma_i(z_i) = 1/(1+e^{-a_i z_i})$, where a_i is the activation potential. The network weights are updated according to the following adaptation laws:

$$\begin{aligned} \dot{\hat{V}} &= -\Gamma_V \left[2\mu e^T \bar{P} b \hat{W}^T \hat{\sigma}' + \lambda \hat{V} \right] \\ \dot{\hat{W}} &= -\Gamma_W \left[2(\hat{\sigma} - \hat{\sigma}' V^T \mu) e^T \bar{P} b + \lambda \hat{W} \right] \end{aligned} \tag{27}$$

where $\hat{\sigma} = \sigma(\hat{V}^T \mu)$ and $\sigma'(x) = diag(d\sigma_i / dz_i)$, e is the tracking error vector, P is the positive definite solution to the Lyapunov equation $A^T \overline{P} + \overline{P}A = -\overline{Q}$ with $\overline{Q} > 0$, A is a Hurwitz matrix, and Γ_V and Γ_W are adaptation gains. It has been shown that the adaptive laws given in Eq. (27) guarantee that all error signals and network weights are uniformly bounded[5].

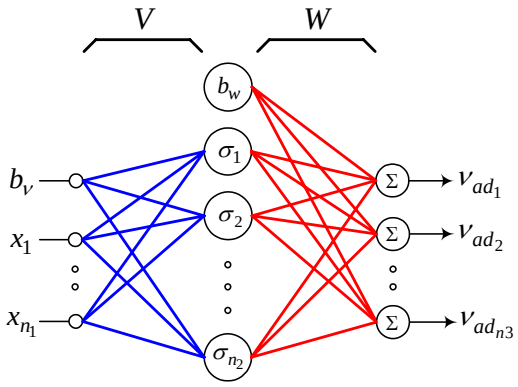

Figure 7. Single Hidden Layer (SHL) perceptron neural network

VII. Simulations

The simulation model was constructed using Matlab/Simulink[13] implementing the UAV's preliminary configuration data, mass property and static wind tunnel data which covers angle of attack from –6 to 20 degrees and sideslip angle from –16 to 16 degrees, along with the assumed dynamic damping derivatives: C_{mq} = –1.0, C_{lp} =–0.25, C_{nr} =–0.1, $C_{m\dot{\alpha}}$ = 0. The aircraft trim conditions are: speed V_T=31.0 m/s, altitude h_T=122.0 m, trim angle of attack α_T=–2.816 degrees, and trim sideslip angle β_T =–0.541 degrees. The trimmed throttle set is 0.44, and it is assumed to be constant during simulations. All aerodynamic control deflections range from –25 to 25 degrees with rate limits of ±120 deg/sec. All simulations begin from this trim condition.

A. Model of Atmospheric Turbulence

The flight envelope of the UAV involves mostly low altitude where gusts or turbulences are common, hence a model of the turbulence needs to be implemented in control simulations. The theory of stochastic processes provides a convenient mean for describing atmospheric turbulence accurately enough for most simulations. For simulation purposes it would be practical to model atmospheric turbulence as white noise passing through a linear filter as shown in Fig. 8, where the relationship between the auto-spectral density of the output signal and the one of the input signal is linear[15].

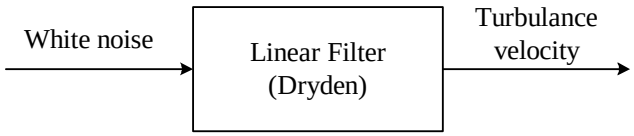

Figure 8. Atmospheric turbulence model as a filtered white noise

Using the Dryden spectra which were developed to approximate the von Karman turbulence spectra by means of rational functions, it is possible to model filters generating turbulence velocity components from white noise inputs. These filters were implemented in the simulation model using Matlab/Simulink.

B. Control Design 1: Two-Stage Dynamic Inversion Based Adaptive Control Design

The control design was carried out assuming that the pilot commands α, β and p_s. The roll channel is relative degree one (r = 1) with respect to the control, while both the α and β channels are relative degree two. The details of this design are written in Ref. 2 and 11.

Since r =1 in the roll channel, a 1st order reference model is employed for that channel, with a time constant of 0.3. Likewise, 2nd order reference models are employed in the pitch and directional channels, with ω_n=5 rad/sec and ζ=1.0. The values selected for the NN gains, defined in Eq.(25), and the number of hidden layer neurons, n_n, are given in Table 1. The activation potentials (a_i) were uniformly distributed between 0.1 and 0.5. In addition, the first NN basis function was used to provide a bias term (a_0 = 0).

Table 1. NN parameters for control design 1.

channel	Γ_V	Γ_W	λ	n_n	n_1	d
P_s	0.5	0.3	0.1	10	5	0.01
α	1.0	1.5	0.1	10	5	0.01
β	0.5	0.5	0.1	10	5	0.01

Angle of Attack Maneuver

Simulation results are presented in Fig. 9-11 for a 12° angle of attack command with zero sideslip and p_s. Figure 9 presents the α, β and p_s responses with and without adaptation (NN/PCH) for the command. As shown in Fig. 9(a), at time 0, α begins from its trim value and initially keeps this value. Subsequently at 5 seconds, a command of 12° is applied. With NN/PCH, α–response follows its reference signal without any overshoot, while β and p_s responses in Fig. 9(b) exhibit oscillations with moderate magnitudes. However, the α–response cannot follow the command without NN/PCH. It can be clearly seen that good tracking is achieved for the vehicle with adaptation.

Time histories of aerodynamic controls for cases with and without adaptation are depicted in Fig. 10. The NN adaptation signal ν_{ad}(t) and inversion error Δ(t) for all channels are compared in Fig. 11. This represents a measure of the degree that adaptation is able to compensate for the inversion error, so it can be seen that NN is presenting its excellent performance all over the simulation period.

Stability Axis Roll Rate (p_s) Maneuver

Simulation results for command of p_s = 150 °/sec while maintaining trim angle of attack are depicted in Fig. 12-14. Figure 12 shows aircraft responses for cases with and without adaptation. It can be seen that good tracking is also maintained in this case with adaptation, except for the transient oscillations in roll response at about 8 and 11 seconds. Without adaptation, α-response diverges at the initial phase.

Figure 13 depicts time histories of aerodynamic controls for cases with and without adaptation. Figure 14 compares $\nu_{ad}(t)$ and $\Delta(t)$ for all three channels. It can be seen that NN compensates for the inversion error precisely.

The simulation results indicate that the UAV has very agile roll maneuverability, and that it can be greatly enhanced by the adaptation.

C. Control Design 2: Command Augmentation based Adaptive Control Design

1. State Feedback

The feedback gains K_1, K_2, K_3, and K_4 in Eq.(12) are chosen in accordance with the following equations:

$$K_2 = K_4 = \frac{\omega_n}{2\zeta}, \qquad K_1 = \tau_n K_2, \qquad K_3 = \tau_y K_4 \tag{26}$$

where

$$\tau_n = \frac{2m}{\rho S V_T C_{L\alpha}}, \qquad \tau_y = \frac{2m}{\rho S V_T \left| C_{y\beta} \right|} \tag{27}$$

The time constants τ, in Eq.(10), for pitch and roll channels, are set to $\tau = 1/2\zeta\omega_n$, and for yaw channel it is set to $\tau = 2/\zeta\omega_n$. The natural frequency(ω_n) and damping ratio(ζ) are set to 5 rad/sec and 2.0, respectively, for simulations. The gains A_1, A_2, A_3 in Eq.(15) are chosen as:

$$A_1 = 25, \quad A_2 = 20, \quad A_3 = 10$$

The values selected for the NN gains and the number of hidden layer neurons, n_n, are given in Table 2. The activation potentials (a_i) were uniformly distributed between 0.1 and 0.5. In addition, the first NN basis function was used to provide a bias term ($a_0 = 0$).

Table 2. Neural network parameters for state and output feedback.

channel	Γ_V	Γ_W	λ	n_n	n_1	d
P	3.0	3.0	0.01	10	5	0.01
Q	3.0	5.0	0.01	10	5	0.01
R	3.0	1.0	0.01	10	5	0.01

Normal Acceleration (a_n) Maneuver

Simulation results using state feedback are presented in Fig. 15-19 for a $1\pm0.8g$ normal acceleration (a_n) command with zero a_y and p. At 4 seconds, a command of 0.2 g is applied and next at 7 seconds, 1.8 g is commanded. Figure 15 presents normal acceleration (a_n), lateral acceleration (a_y) and roll rate (p) responses with and without adaptation (NN/PCH) for the command. As shown in Fig. 15(a), a_n follows its command with little overshoots with adaptation. The roll rate (P) and lateral acceleration (a_y) shown in Fig. 15(b) are maintained very close to zero command with adaptation, except for the short periods of transient response. It is noted that, without adaptation, normal acceleration, a_n shows bigger overshoot, and P and a_y responses are not kept zero as commanded and they even diverge from commanded zeros along with yaw rate (R) in Fig.16. These results are highly undesirable. Pitch rate (Q) and yaw rate (R), presented in Fig. 16, follow the reference signals with adaptation. Angle of attack and sideslip angle are depicted in Fig. 17, and they show difficulty in returning to trim conditions without adaptation. Time histories of control deflections are presented in Fig. 18, and it is noted that PCH is activated for elevator at right after 4 and 7 seconds because of the actuator rate limits. The NN adaptation signal ν_{ad}(t) and inversion error Δ(t) for all channels are compared in Fig. 19. It can be seen that NN output, ν_{ad}(t) is nicely canceling out the error Δ(t) all over the simulation period.

Roll Rate (*P*) Maneuver

Simulation results using state feedback for command of P = $\pm$150 ^{o}/sec, while maintaining 1.0 g a_n and zero a_y, are depicted in Fig. 20-24. At 4 seconds, a command of +150 ^{o}/sec is applied and next at 7 seconds, -150 ^{o}/sec g is commanded. Figure 20(a) shows roll rate response for cases with and without adaptation. It can be seen that good tracking is maintained with adaptation, while it shows bigger error without adaptation. Normal and lateral accelerations are depicted in Fig. 20(b) and they follow the commanded values, one and zero, respectively. Pitch rate (Q) and yaw rate (R) are presented in Fig. 21, where it can be seen that Q and R follow the reference signals even without adaptation. Angle of attack (α) and sideslip angle (β) are depicted in Fig. 22, and β shows bigger transient amplitude with adaptation. Figure 23 shows time histories of control deflections, and the NN adaptation signal ν_{ad}(t) and inversion error Δ(t) for all channels are compared in Fig. 12. It can be seen that NN is showing good adaptation.

2. Output Feedback

The same parameter settings and NN gains in Table 2 as those for state feedback in previous subsection are used for output feedback case, except for using Eq.(16) instead of Eq.(13). As noted in earlier section, it is assumed that α and β are not available.

Normal Acceleration (a_n) Maneuver

Simulation results using output feedback are presented in Fig. 25-29 for a $1\pm0.8g$ normal acceleration (a_n) command with zero a_y and p. Likewise state feedback case, at 4 seconds, a command of 0.2 g is applied and next at 7 seconds, 1.8 g is commanded. Figure 25 presents a_n, a_y and p responses with and without adaptation (NN/PCH) for the command. Pitch rate (Q) and yaw rate (R), presented in Fig. 26, follow the reference signals with adaptation. Angle of attack and sideslip angle are depicted in Fig. 27. Overall responses for this command are similar to those of state feedback case. Time histories of control deflections are presented in Fig. 28, and the NN adaptation signal $\nu_{ad}(t)$ and inversion error $\Delta(t)$ for all channels are compared in Fig. 29. It can also be seen that NN output, $\nu_{ad}(t)$ shows good adaptation by nicely canceling out the error $\Delta(t)$ all over the simulation period.

Roll Rate (*P*) Maneuver

Simulation results using output feedback for command of P = ±150 °/sec, while maintaining 1.0 g a_n and zero a_y, are depicted in Fig. 30-34. Likewise state feedback case shown in previous subsection, at 4 seconds, a command of +150 °/sec is applied and next at 7 seconds, -150 °/sec g is commanded. Figure 30(a) shows roll rate response for cases with and without adaptation. Normal and lateral accelerations are depicted in Fig. 20(b), and pitch rate (Q) and yaw rate (R) are presented in Fig. 31. Angle of attack (α) and sideslip angle (β) are depicted in Fig. 32. Like the normal acceleration maneuver, the overall responses of this command are also similar to those of state feedback case. Figure 33 shows time histories of control deflections, and the NN adaptation signal $\nu_{ad}(t)$ and inversion error $\Delta(t)$ for all channels are compared in Fig. 34. It can be seen that NN is showing good adaptation by canceling out the error $\Delta(t)$ in each channel.

VIII. Conclusion

Two NN-based adaptive control designs for the FQM-117B UAV are discussed: One with two-stage dynamic inversion with state feedback, and the other with a feedback dynamic inversion based on a command augmentation system with state and output feedback. The tracking performances of both approaches are greatly improved by the NN-based adaptive control design, thereby implying adaptation to modeling error and uncertainties. Pseudo-control hedging is implemented to protect the adaptive process during periods of control nonlinearities such as position limits and rate limits.

Acknowledgments

This research was supported by NASA Grant No. NAG-1-01117.

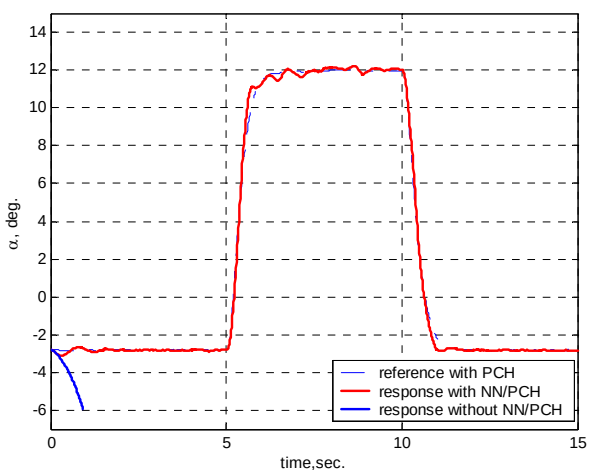

(a) Angle of attack

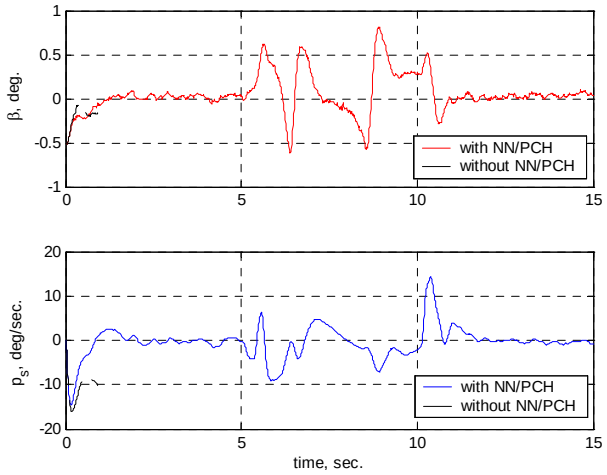

(b) Sideslip angle and stability axis roll rate

Figure 9. Aircraft responses for an α–command with/without NN adaptation.

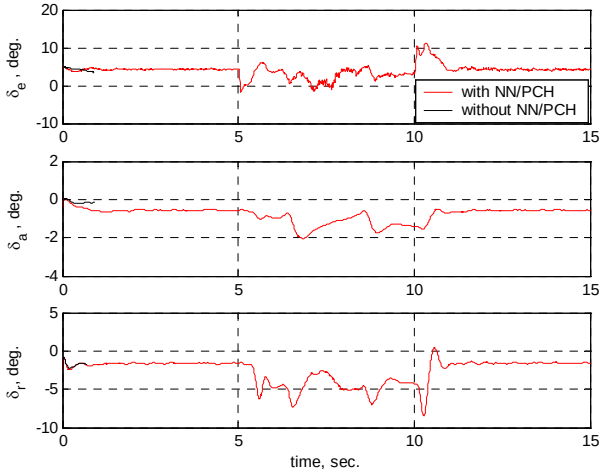

Figure 10. Aerodynamic control defections

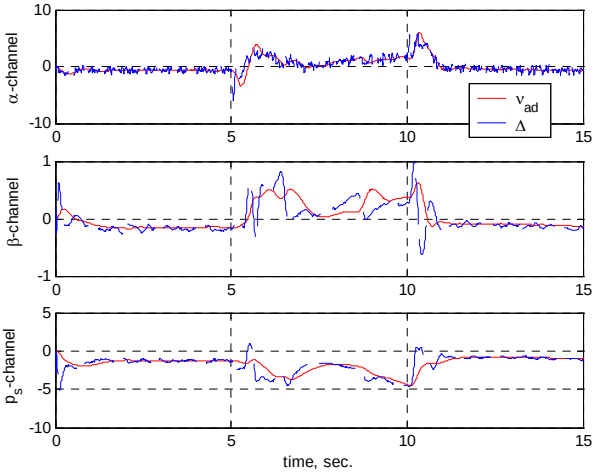

Figure 11. NN adaptation signal ν_{ad}(t) and Δ(t)

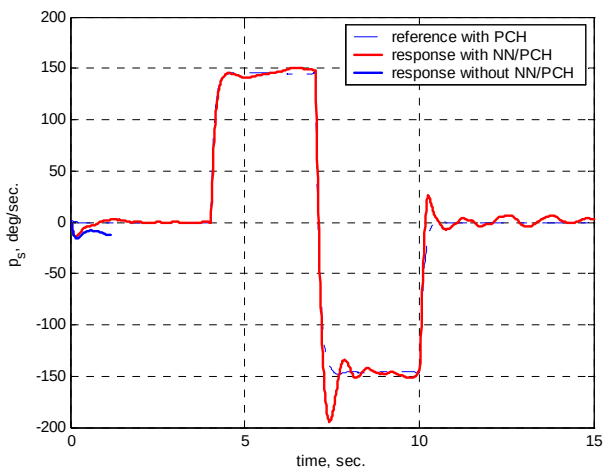

(a) Stability axis roll rate

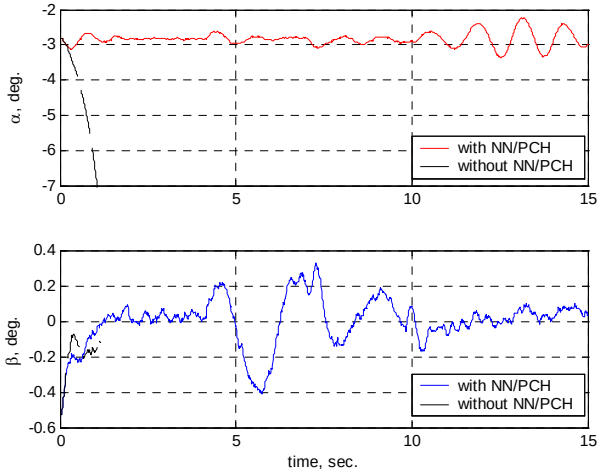

(b) Angle of attack and sideslip angle

Figure 12. Aircraft responses for a p_s-command with/without NN adaptation.

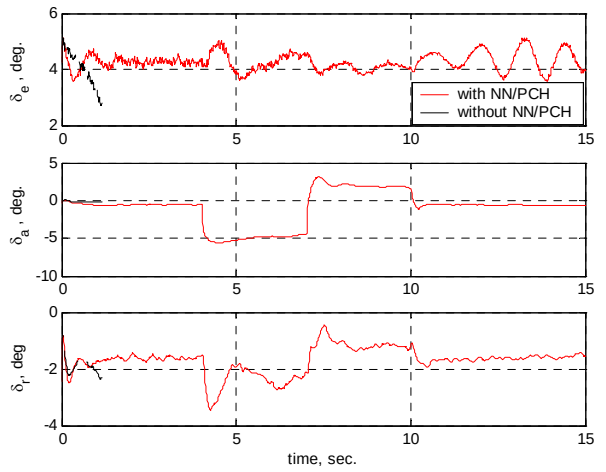

Figure 13. Aerodynamic control defections.

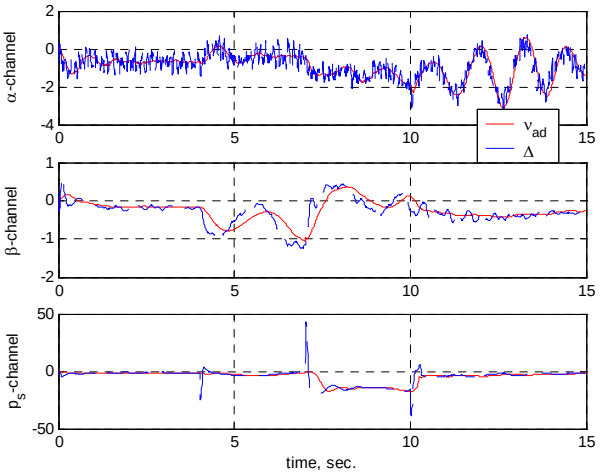

Figure 14. NN adaptation signal ν_{ad}(t) and Δ(t)

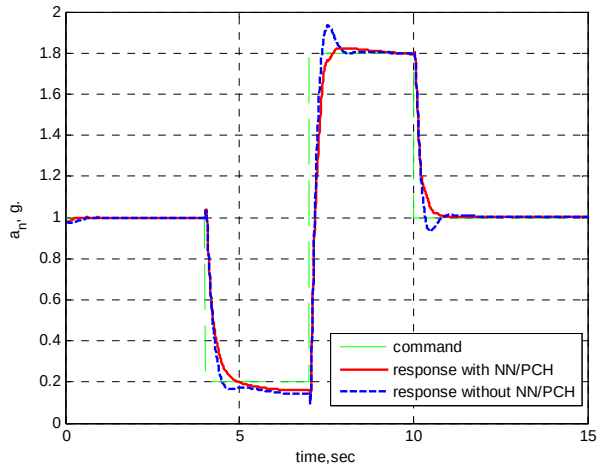

(a)Normal acceleration (a_n)

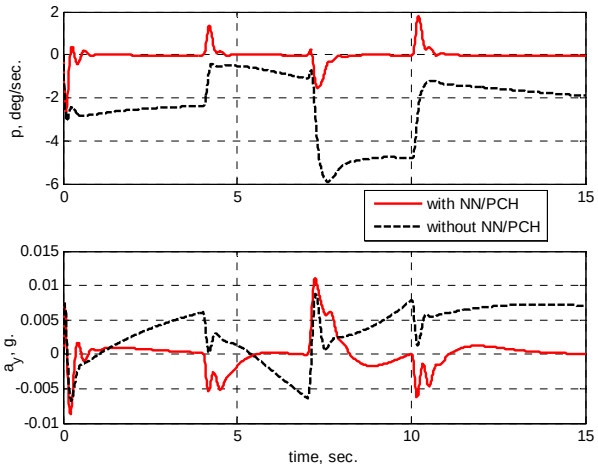

(b) Roll rate (P) and lateral acceleration (a_y)

Figure 15. Aircraft responses for a normal acceleration (a_n) command using state feedback with/without NN adaptation.

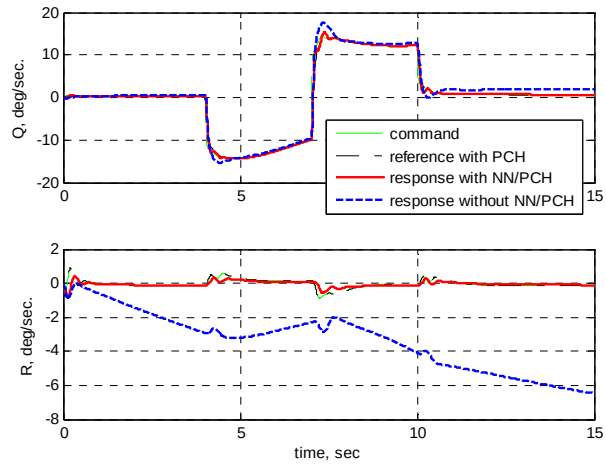

Figure 16. Pitch Rate, Q and Yaw Rate, R.

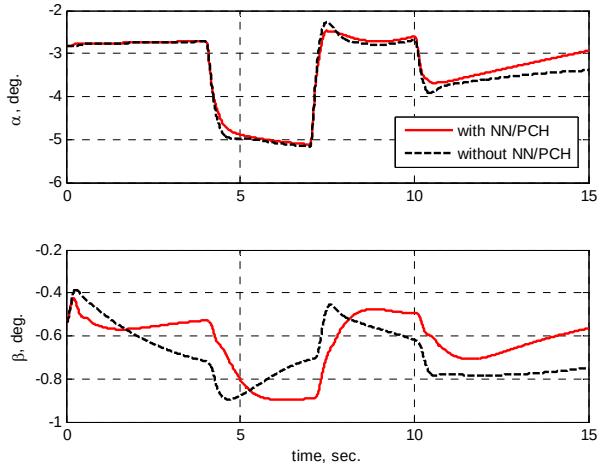

Figure 17. Angle of attack and sideslip angle.

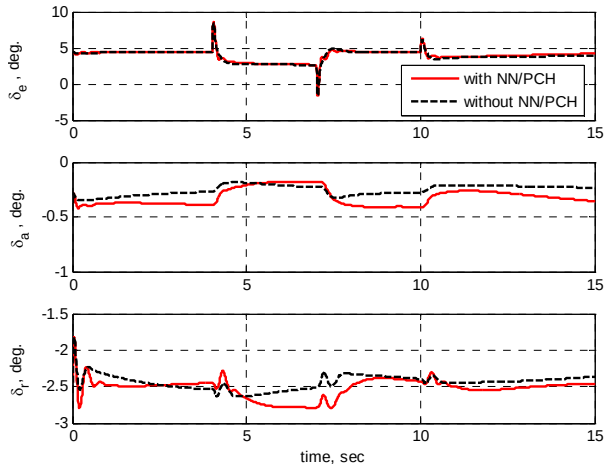

Figure 18. Aerodynamic control defections.

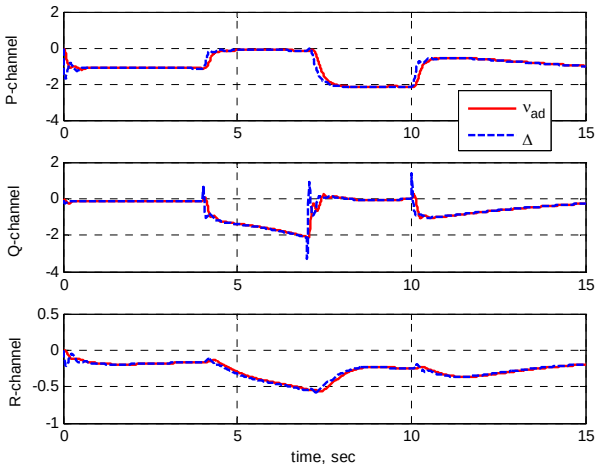

Figure 19. NN adaptation signal $\nu_{ad}(t)$ and $\Delta(t)$.

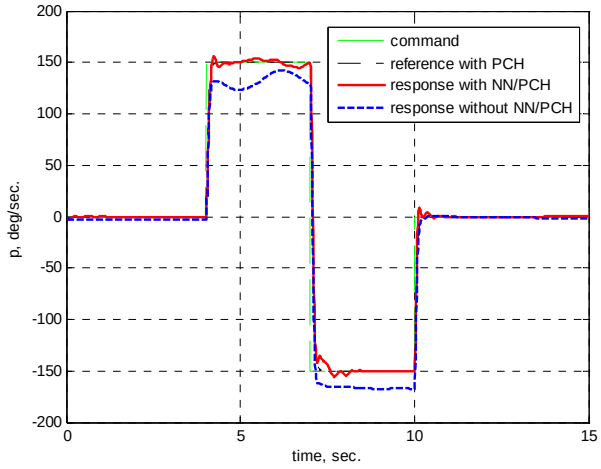

(a) Roll rate (P)

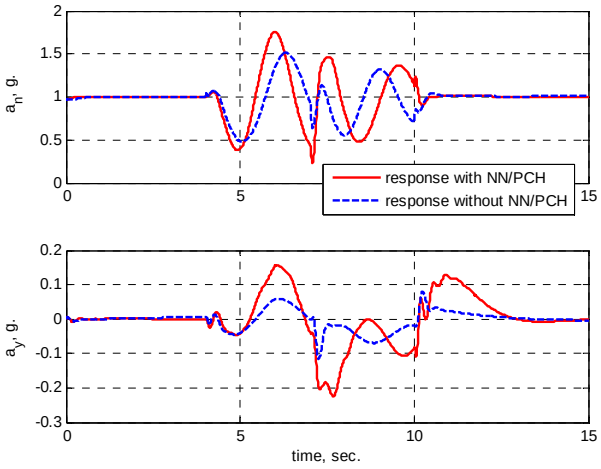

(b) Normal acceleration (a_n) and lateral acceleration (a_y)

Figure 20. Aircraft responses for a roll rate (P) command using state feedback with/without NN adaptation.

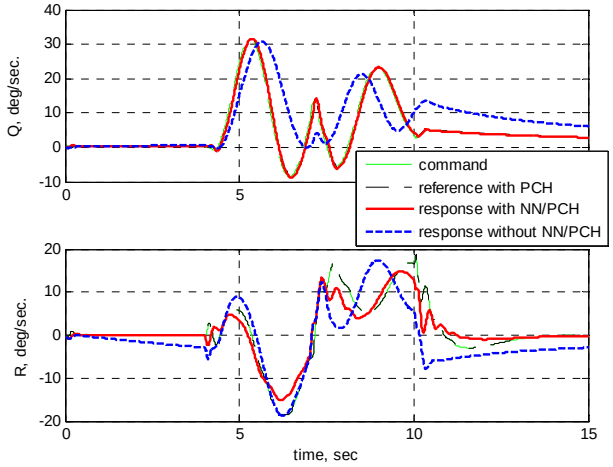

Figure 21. Pitch Rate, Q and Yaw Rate, R.

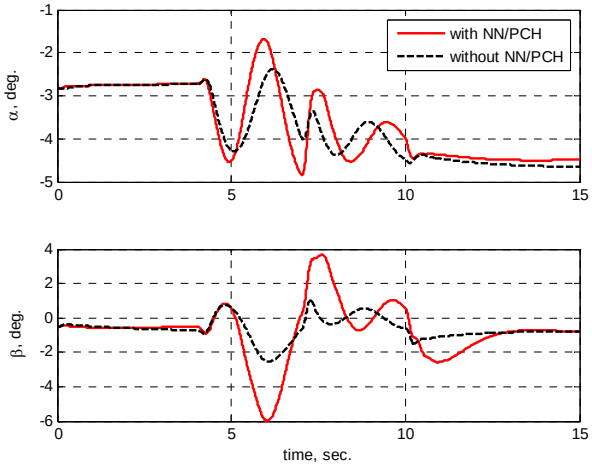

Figure 22. Angle of attack and sideslip angle.

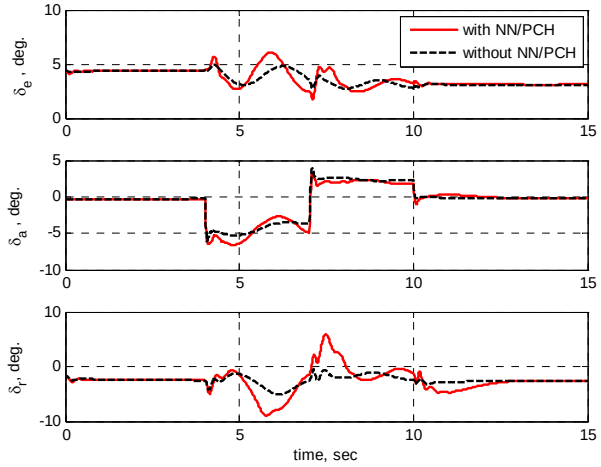

Figure 23. Aerodynamic control defections.

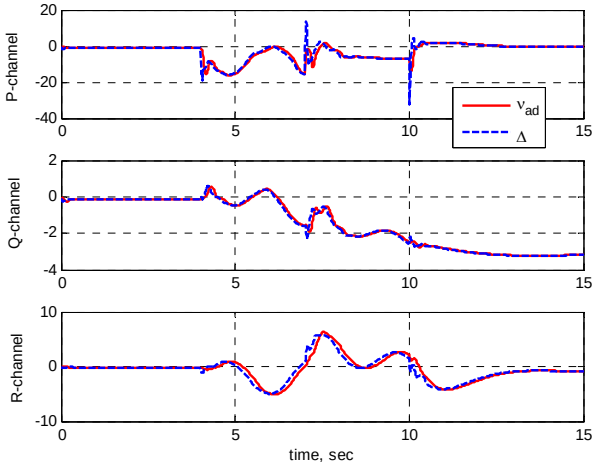

Figure 24. NN adaptation signal $\nu_{ad}(t)$ and $\Delta(t)$.

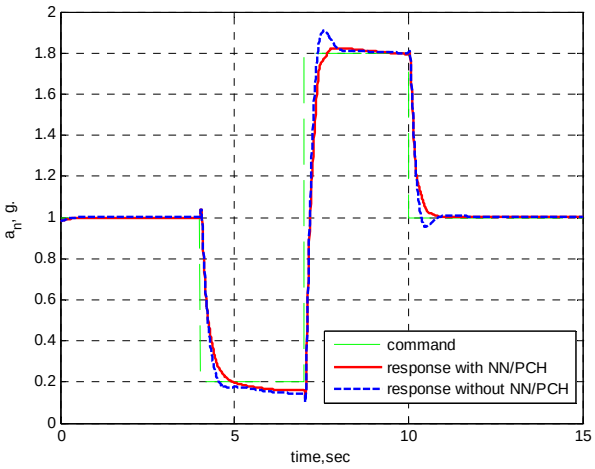

(a)Normal acceleration (a_n)

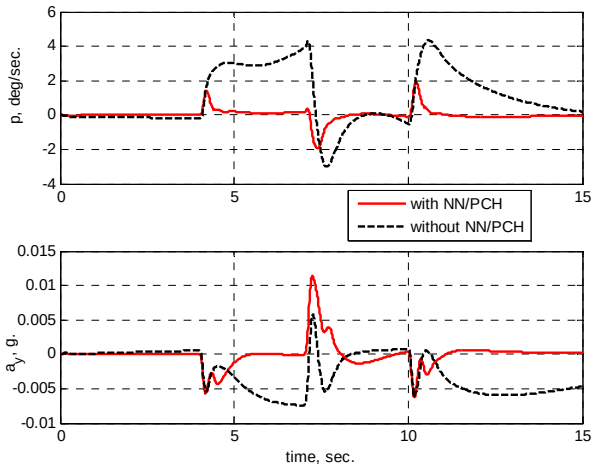

(b) Roll rate (P) and lateral acceleration (a_y)

Figure 25. Aircraft responses for a normal acceleration (a_n) command using output feedback with/without NN adaptation.

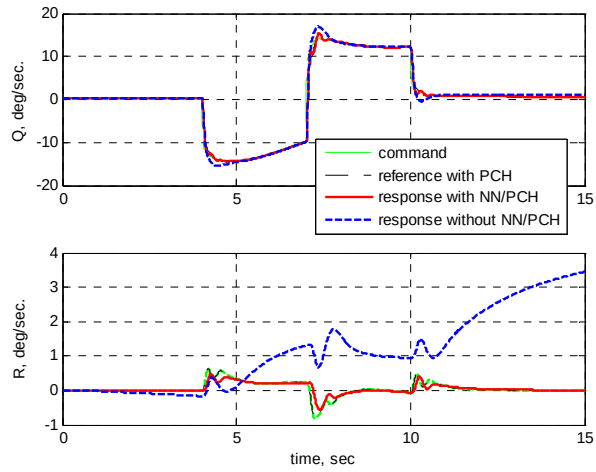

Figure 26. Pitch Rate, Q and Yaw Rate, R.

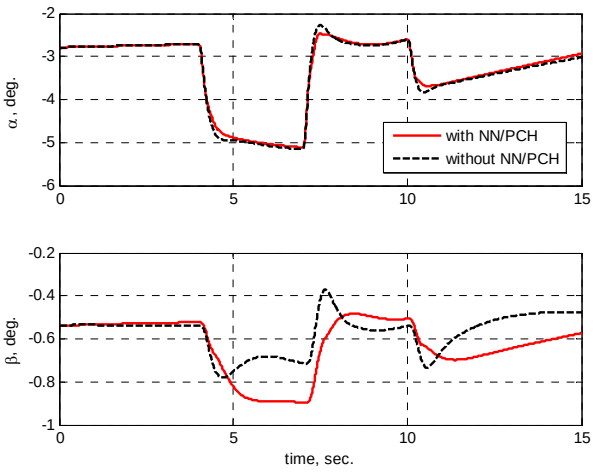

Figure 27. Angle of attack and sideslip angle.

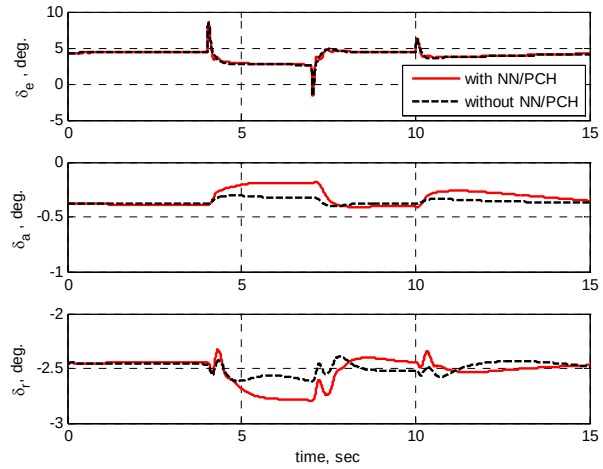

Figure 28. Aerodynamic control defections.

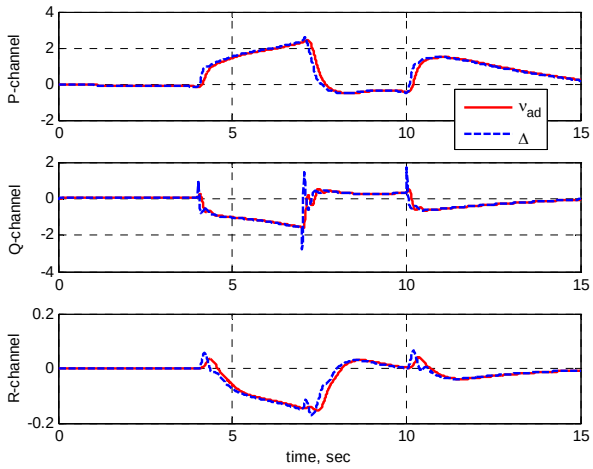

Figure 29. NN adaptation signal $\nu_{ad}(t)$ and $\Delta(t)$.

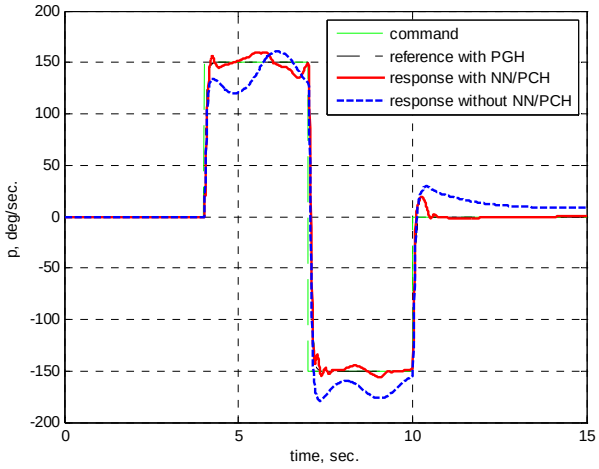

(a) Roll rate (P)

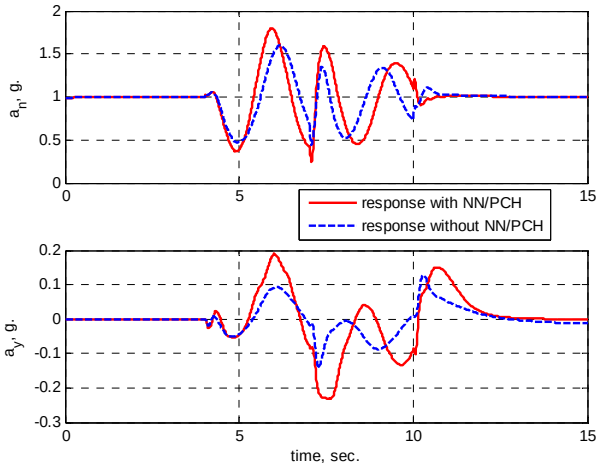

(b) Normal acceleration (a_n) and lateral acceleration (a_y)

Figure 30. Aircraft responses for a roll rate (P) command using output feedback with/without NN adaptation.

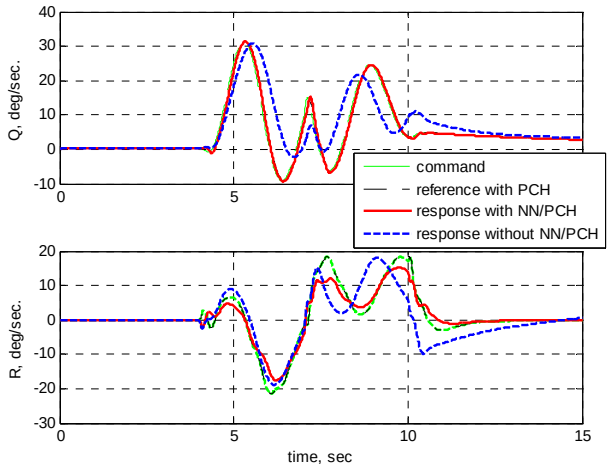

Figure 31. Pitch Rate, Q and Yaw Rate, R.

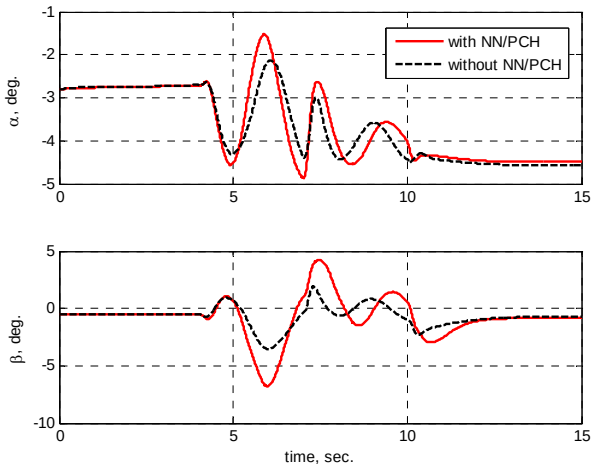

Figure 32. Angle of attack and sideslip angle.

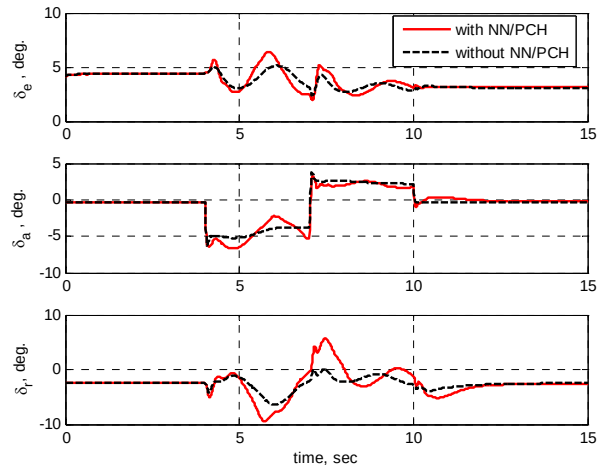

Figure 33. Aerodynamic control defections.

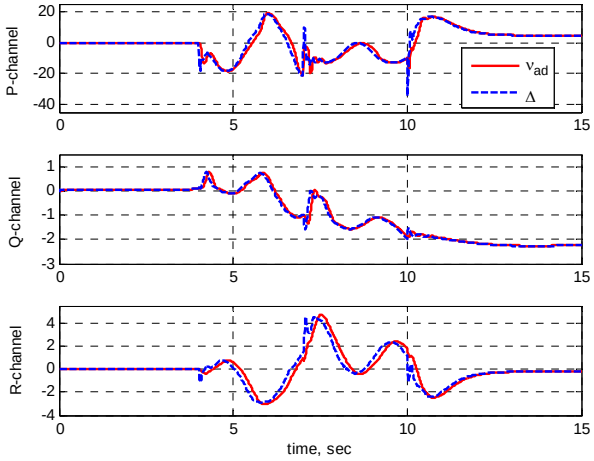

Figure 34. NN adaptation signal $\nu_{ad}(t)$ and $\Delta(t)$.

References

[1]Calise, A.J., Lee, S., Sharma, M., "Development of a Reconfigurable Flight Control Law for Tailless Aircraft," *Journal of Guidance, Control and Dynamics*, Vol. 24, No.5, 2001, pp.896-902.

[2]Shin, Y., Johnson, M., and Calise, A., "Neural Network-Based Adaptive Control for Nonlinear Flight Regimes", *AIAA Guidance, Navigation and Control Conference*, Austin, TX, August 2003.

[3]Calise, A., Shin Y., Johnson, M., "Comparison Study of Conventional and Neural Network Based Adaptive Control of Wing Rock", *AIAA Guidance, Navigation and Control Conference*, Providence, RI, August 2004.

[4]Calise, A. J., Hovakimyan, N. and Idan, M., "Adaptive Output Feedback Control of Nonlinear Systems Using Neural Networks" *Automatica*, August, 2001.

[5]Hovakimyan, N., Nardi, F., Calise, A.J., Kim, N., "Adaptive Output Feedback Control of Uncertain Systems using Single Hidden Layer Neural Networks," IEEE Transactions on Neural Networks. 2001.

[6]Johnson, E., Calise, A.J., "Neural Network Adaptive Control of Systems with Input Saturation", *American Controls Conference*, Arlington, Virginia, June, 2001.

[7]Motter, Mark A., "Autonomous Flight Tests of a Small Unmanned Aerial Vehicle", NASA Langley Research Center, Virginia.

[8]Aviation Publishing, Aviation Flight Manuals and Accessories, TM-9-1550-416-14P, "Operator, Unit and Intermediate Direct and General Support Maintenance Manual Including Repair Parts and Special Tools LIS for FQM-117 B-1 and C-1 Radio Controlled Miniature Aerial Target (RCMAT) Ground Support Equipment, and Auxiliary Equipment", http://www.tpub.com/content/aviationandaccessories/TM-9-1550-416-14P/

[9]Brinker, J.S., Wise, K.A., "Stability and Flying Qualities Robustness of a Dynamic Inversion Aircraft Control Law," *Journal of Guidance, Control and Dynamics*, Vol. 19, No.6, 1996, pp.1270-1277.

[10]Adams, R.J., Buffington, J.M., Banda, S.S., "Design of Nonlinear Control Laws for High Angle of Attack Flight," *Journal of Guidance, Control and Dynamics*, Vol. 17, No.4,1994, pp.737-746.

[11]Calise, A.J., Shin, Y., Johnson, M., "Neural Network-Based Adaptive Control for Nonlinear Flight Regimes" NASA Technical Report, August, 2002 and 2003.

[12]Menon, P., "Nonlinear Command Augmentation System for a High Performance Aircraft," Proceedings of the AIAA Guidance, Navigation and Control Conference, 1993, pp. 720-730.

[13]Rauw, M., "FDC 1.2. A Simulink Toolbox for Flight Dynamics and Control Analysis" 2nd edition, May 10, 2001.